NANO LETTERS

pubs.acs.org/NanoLett

Nanoassembled Plasmonic-Photonic Hybrid Cavity for Tailored Light-Matter Coupling

Michael Barth,[†] Stefan Schietinger,[†] Sabine Fischer,[†] Jan Becker,[‡] Nils Nüsse,[§] Thomas Aichele,[†] Bernd Löchel,[§] Carsten Sönnichsen,[‡] and Oliver Benson*[,†]

[†]Institute of Physics, Humboldt-Universität zu Berlin, Hausvogteiplatz 5−7, D-10117 Berlin, Germany, [‡]Institute for Physical Chemistry, University of Mainz, Jakob-Welder-Weg 11, D-55128 Mainz, Germany, and [§]Application Centre for Microengineering, Helmholtz-Centre Berlin for Materials and Energy, Albert-Einstein-Strasse 15, D-12489 Berlin, Germany

ABSTRACT We propose and demonstrate a hybrid cavity system in which metal nanoparticles are evanescently coupled to a dielectric photonic crystal cavity using a nanoassembly method. While the metal constituents lead to strongly localized fields, optical feedback is provided by the surrounding photonic crystal structure. The combined effect of plasmonic field enhancement and high quality factor ($Q \approx 900$) opens new routes for the control of light-matter interaction at the nanoscale.

KEYWORDS Photonic crystal cavities, plasmonic nanostructures, nanoassembly

The ability to confine light into ultrasmall volumes is essential for enhancing the interaction of light and matter in the emerging field of nanophotonics. Surface plasmons[1] provide a route to such strong optical confinement in the subwavelength regime and are of high interest for (cavity) quantum electrodynamics applications.[2,3] They are bound electromagnetic excitations at the interface between a metal and a dielectric, resulting from collective electron oscillations at the surface of the metal. Because of their ability to concentrate electromagnetic energy in volumes much smaller than the corresponding wavelength, they provide a very strong interaction between (quantum) emitters and photon fields.[2] This interaction can further be enhanced through an appropriate feedback mechanism, provided, for example, by cavity structures. Various types of such plasmonic cavities have already been realized,[4−7] exhibiting mode volumes V_{eff} down to $\approx$100 nm^3 (ref 5), but the achieved quality factors Q were limited to values <100 due to losses in the metal. Only recently a plasmonic microdisk cavity with $Q \approx 1000$ was demonstrated in the near-infrared,[8] but at the expense of a larger mode volume $V_{\mathrm{eff}} \approx 2.5\,\mu\mathrm{m}^3$. On the other hand, dielectric or semiconductor microcavities can reach high quality factors and small mode volumes,[9] but the achievable field localization is inherently limited by the laws of diffraction.[10]

In this letter, we report the realization and characterization of a hybrid photonic crystal (PhC) cavity that combines the benefits of both plasmonic and photonic elements. Contrary to previous designs where a dielectric or semiconducting core was completely coated with a metal layer,[7,8] we use individual metal nanoparticles that are deterministically placed on the dielectric backbone of a PhC cavity. This type of hybrid structure can exhibit both high quality factors and pronounced hot spot of the electromagnetic field, potentially enhancing the interaction of the cavity mode with emitters or other types of active materials. This approach is fundamentally different from the system recently introduced by de Angelis et al.,[11] where the actual cavity mode was strongly damped due to the presence of a metal nanowire. In the system studied here the original cavity characteristics are preserved and extended by plasmonic features. This allows for a coherent coupling of the photonic and plasmonic resonances and constitutes a novel class of hybrid nanophotonic devices.[12]

As the dielectric building block of the hybrid device we employ a planar double-heterostructure PhC cavity[13,14] made from silicon nitride. It consists of a PhC waveguide (one row of missing holes) that is locally modulated by enlarging the lattice constant $a = 270$ nm to $a' = 280$ nm over two lattice periods to create an optical potential well. Details of the fabrication method were published elsewhere.[15] The properties of this cavity (shown schematically in Figure 1a) are probed by monitoring the intrinsic fluorescence of the silicon nitride membrane, which is excited using a frequency-doubled Nd:YAG laser (532 nm wavelength, $\sim$100 μW excitation power). The polarization of the excitation light is controlled via a $\lambda/2$ waveplate. The emission is collected perpendicular to the PhC membrane through a 100 × /0.9 NA microscope objective, spectrally dispersed by a spectrograph (focal length 500 mm) and detected with a liquid nitrogen cooled CCD camera. A 100 μm pinhole in the detection path is used for spatial filtering of the cavity emission.

* To whom correspondence should be addressed: E-mail: oliver.benson@physik.hu-berlin.de.

Received for review: 10/23/2009
Published on Web: 02/08/2010

DOI: 10.1021/nl903555u | *Nano Lett.* **2010,** *10,* 891–895

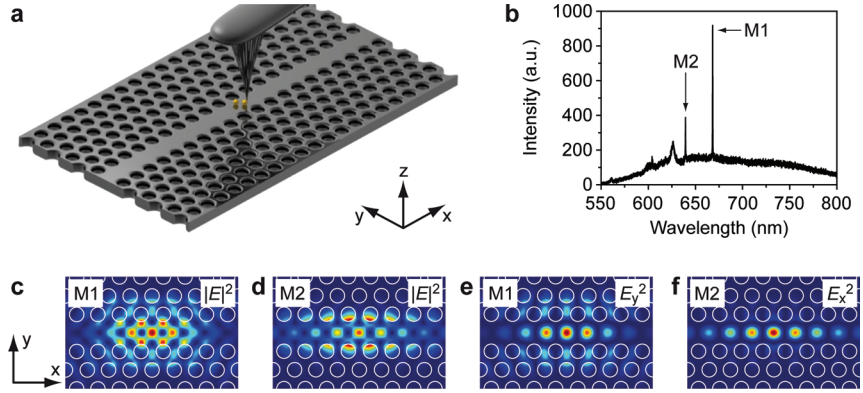

FIGURE 1. (a) Illustration of the PhC cavity and the employed AFM manipulation technique. (b) Spectrum of the intrinsic fluorescence from a silicon nitride PhC cavity (with hole radii $r = 0.28a$ and a membrane thickness $t = 200$ nm), exhibiting sharp resonances associated with the cavity modes M1 and M2. (c,d) Calculated in-plane electric field intensity distributions $|E|^2$ of modes M1 (c) and M2 (d), respectively. (e,f) Corresponding plots of the dominant electric field component at the center of the cavity, which is E_y^2 in the case of mode M1 (e) and E_x^2 in the case of mode M2 (f).

A typical fluorescence spectrum from such a PhC cavity is displayed in Figure 1b, exhibiting two sharp resonance peaks associated with the two lowest cavity modes, denoted as M1 and M2. The corresponding electric field intensity distribution $|E|^2$ for both modes, obtained from three-dimensional finite-difference time-domain (FDTD) simulations, is displayed in Figure 1c,d, respectively. Note that M1 and M2 are polarized orthogonal to each other at the center of the cavity, as can be seen from the plots of the dominant field polarization (E_y for M1 and E_x for M2) in Figure 1e and Figure 1f, respectively.

To realize the hybrid cavity system we use a modified dip-pen technique[16] in combination with atomic force microscope (AFM) manipulation.[17−19] The end of a tapered fiber (tip radius ≈ 1 μm) is dipped into a solution of chemically grown gold nanoparticles and brought into contact with the silicon nitride surface near the PhC structure. In this way, small particle reservoirs are created, from which individual gold nanoparticles can be selected and moved into the cavity (along the PhC waveguide) using the tip of an AFM[20] (see Figure 1a for illustration). Thereby, the accuracy in positioning the particles is ~10 nm. Compared to lithographically fabricated metal structures, which suffer from a limited spatial resolution and a high degree of polycrystallinity, this manipulation procedure allows the assembly and rearrangement of very small plasmonic structures of high quality, that is, relatively low damping.[21] Furthermore, it provides consistency between measurements, as the very same constituents can be studied in different spatial configurations.

We start our investigation with a system of a single gold nanorod placed upon the center of the cavity. The PhC structure employed for this purpose exhibits hole radii $r = 0.28a$ and resonance wavelengths of 668 and 640 nm for mode M1 and M2, respectively. The gold nanorods were synthesized in batch by the seed-mediated growth technique.[22] Their extinction spectrum and a transmission electron microscope image are shown in Figure S1 of the Supporting Information. Two different configurations are

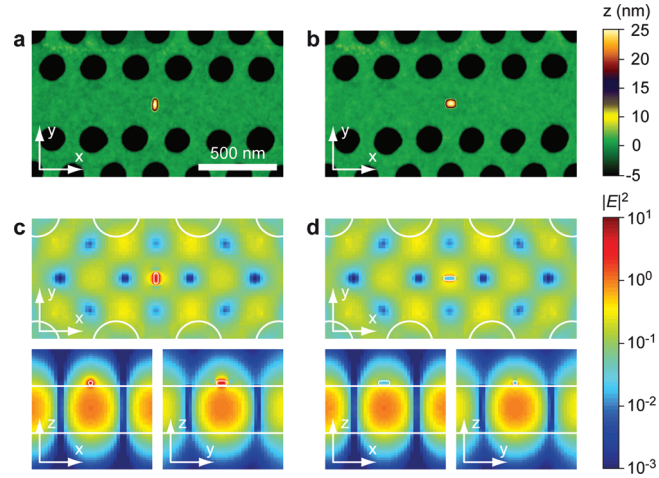

FIGURE 2. (a,b) AFM images of a PhC cavity with a gold nanorod placed on top of its center in different orientations. The nanorod appears in a slightly different aspect ratio in both images due to the convolution with the shape of the AFM tip. (c,d) Corresponding calculated electric field intensity distributions $|E|^2$ (for mode M1) of the configurations shown in (a) and (b), respectively. Each panel displays x-y, x-z, and y-z cross sections through the center of the gold nanorod. The logarithmic color scale is always normalized to the respective $|E|^2$ value at the center of the PhC slab.

realized, with the gold nanorod (diameter ≈ 20 nm, length ≈ 50 nm) being either oriented perpendicular (Figure 2a) or parallel (Figure 2b) to the waveguide axis. Corresponding FDTD simulations of the electric field intensity distribution $|E|^2$ for mode M1 are shown in Figure 2c and Figure 2d, respectively. Apparently, the cavity field couples to the plasmonic resonance of the nanorod, leading to a shift of the field maximum from the center of the PhC slab to its surface. This effect is particularly pronounced if the nanorod orientation matches the field polarization, as is the case for mode M1 in Figure 2c. The shifted field distribution is highly advantageous for all applications where external emitters or other types of materials placed on top of the PhC structure have to be coupled evanescently to the cavity mode.

DOI: 10.1021/nl903555u | *Nano Lett.* **2010,** *10,* 891−895

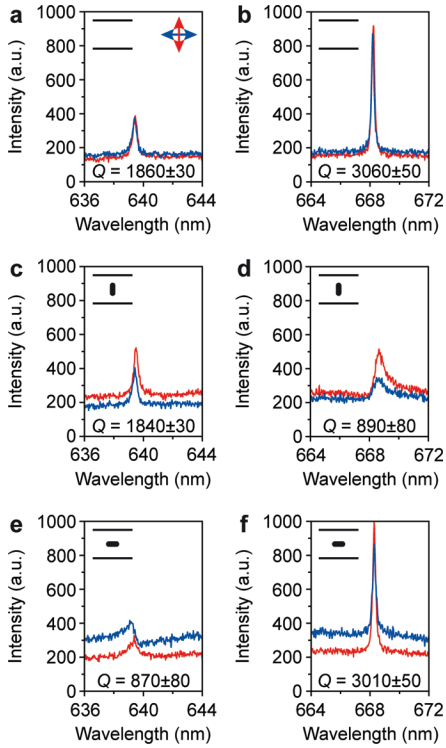

FIGURE 3. (a,b) Resonance peaks of modes M2 (a) and M1 (b) for the bare cavity (without nanorod). Red and blue curves refer to excitation polarizations perpendicular and parallel to the waveguide axis, respectively. (c,d) Resonance peaks of modes M2 (c) and M1 (d) for the configuration shown in Figure 2a (see inset). (e,f) Resonance peaks of modes M2 (e) and M1 (f) for the configuration shown in Figure 2b (see inset). The quality factor Q for each resonance is determined by fitting either a Lorentzian or a Fano-type function (eq 3) to the data. A slightly increased fluorescence intensity is observed when the excitation polarization matches the orientation of the gold nanorod, resulting from a plasmonic enhancement of the nanorod emission.

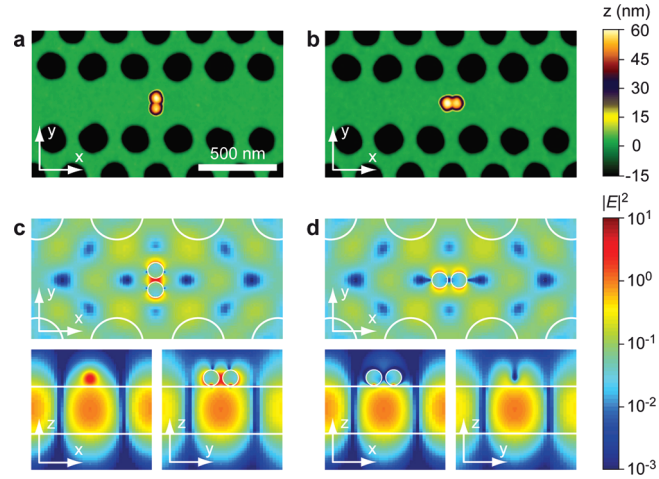

FIGURE 4. (a,b) AFM images of a PhC cavity with two gold nanospheres placed on top of its center and aligned in different orientations. The gap between the spheres is (15 ± 5) nm (a) and (5 ± 5) nm (b), respectively. (c,d) Corresponding calculated electric field intensity distributions $|E|^2$ (for mode M1) of the configurations shown in (a) and (b), respectively. Each panel displays x-y, x-z, and y-z cross sections through the center of the gold dimer. The gap between the two nanospheres is chosen as 20 nm. The logarithmic color scale is always normalized to the respective $|E|^2$ value at the center of the PhC slab.

To study the impact of the gold nanorod on the quality factor Q of the cavity, the resonance spectra of modes M1 and M2 are measured and displayed in Figure 3. Clearly, the quality factor is reduced to values $Q \approx 900$ for both modes when the nanorod is oriented parallel to the corresponding mode polarization (Figure 3d,e) due to increased scattering and absorption in the metal. Thereby, the asymmetric, Fano-type[23] line shape results from interference effects of light scattered or radiated directly from the nanorod and light reaching the detector on other pathways. This effect is discussed in more detail below. Surprisingly, the quality factor and line shape is nearly unaffected when the nanorod is oriented perpendicular to the mode polarization (Figure 3c,f), indicating a very weak coupling between the photonic and plasmonic resonance. As the modes M1 and M2 are polarized orthogonal to each other at the center of the cavity (see Figure 1e,f), the nanorod couples either to M1 or M2, depending on its orientation. This opens interesting possibilities to tailor the light-matter coupling, for example, by creating a system which can be efficiently excited at the wavelength of the plasmon-coupled mode (with lower Q, but high plasmonic field enhancement) and emits at the wavelength of the unaffected mode (with high Q), or vice versa. Such a system provides an ideal platform, for example, to generate and harvest single photons with high efficiency, as the interaction of the emitter with the excitation field is strongly increased,[24] while a narrow-band emission channel exists to collect and distribute the generated photons.

Next, we consider a more complex metal structure, that is, a plasmonic nanoantenna consisting of two gold nanospheres (~60 nm in diameter, provided by BBInternational). A different PhC cavity is employed for this purpose, exhibiting hole radii $r = 0.34a$ and resonance wavelengths 638 and 604 nm for mode M1 and M2, respectively. The nanoantenna is either aligned perpendicular (Figure 4a) or parallel (Figure 4b) to the waveguide axis. Again, the corresponding electric field intensity distribution $|E|^2$ for mode M1 is shown in Figure 4c,d, respectively. When the alignment direction of the gold nanospheres matches the field polarization (Figure 4c), a pronounced hot spot is created in the gap between them, which increases in strength with decreasing sphere separation.[25] In the example shown in Figure 4c,d, a moderate gap size of 20 nm is chosen, allowing active materials (e.g., quantum emitters such as defect centers in diamond nanocrystals[19,20]) to be inserted into this gap. The calculated $|E|^2$ value at the center $\vec{r}_0$ between the spheres is still 22 times higher than that of the bare PhC cavity, potentially enhancing the interaction of the cavity field with a quantum emitter located at $\vec{r}_0$.

The enhancement effect can be expressed in terms of the cavity Purcell factor[26]

DOI: 10.1021/nl903555u | Nano Lett. 2010, 10, 891–895

$$F = \frac{3}{4\pi^2}\left(\frac{\lambda}{n}\right)^3 \frac{Q}{V_{\text{eff}}} \tag{1}$$

where V_{eff} is the effective mode volume defined as

$$V_{\text{eff}} = \frac{\int \varepsilon(\vec{r})|\vec{E}(\vec{r})|^2 \mathrm{d}\vec{r}}{\varepsilon(\vec{r}_0)|\vec{E}(\vec{r}_0)|^2} \tag{2}$$

Here, $\varepsilon(\vec{r})$ is the real part of the dielectric constant. Note that this definition of the mode volume differs from the one usually employed, where max $\{\varepsilon(\vec{r})|\vec{E}(\vec{r})|^2\}$ appears in the denominator of eq 2 instead of $\varepsilon(\vec{r}_0)|\vec{E}(\vec{r}_0)|^2$. This, however, would result in unrealistically small mode volumes due to the extremely high local field intensities occurring at certain points near the metal surface. Consequently, we use the fixed reference point $\vec{r}_0$ for all calculations, in this way automatically accounting for a reduced emitter-cavity coupling when the emitter is not placed at the field maximum of the cavity mode. From the calculated field distribution shown in Figure 4d we deduce a reduction of V_{eff} by a factor of 34 compared to the bare PhC cavity. Together with the experimental quality factor, which is reduced from $Q = 2500$ to $Q = 720$ in the presence of the nanoantenna, this still yields an ~10 times net enhancement of the Purcell factor according to eq 1. Details on the effective mode volume, quality factor, and Purcell enhancement of other gold-cavity configurations are provided in Charts S1 and S2 of the Supporting Information.

To probe the modal properties experimentally, we exploit the intrinsic plasmon-enhanced emission of the gold nanospheres as an internal light source.[27] For a single gold particle this emission is weak compared to the background fluorescence from the silicon nitride membrane. However, if the two nanospheres are brought together and excited along their alignment axis, a strong increase of the fluorescence signal occurs (see Figure 5a) due to the hot spot formation discussed above, accompanied by a redshift of the plasmon resonance from ~540 nm to wavelengths >600 nm, depending on the exact distance between the spheres.[28,29] The plasmon-enhanced emission is strongly polarized in the alignment direction of the nanospheres and clearly dominates over the background fluorescence from the silicon nitride, allowing us to study the coherent interaction between the nanoantenna and the cavity mode. This interaction is manifested in the pronounced Fano-like line shape[23] observed in the spectrum in Figure 5a. It results from an interference of the two possible pathways on which a photon emitted by the source (i.e., the nanoantenna) can reach the detector, namely directly through emission into a continuum of extended free-space modes or resonantly through emission into the cavity mode and subsequent outcoupling to free-space modes. Note that a pronounced Fano effect is only produced when the polarization of the source and that of the radiation from the cavity mode coincide, as can be seen from the polarization-resolved spectra in Figure 5b.

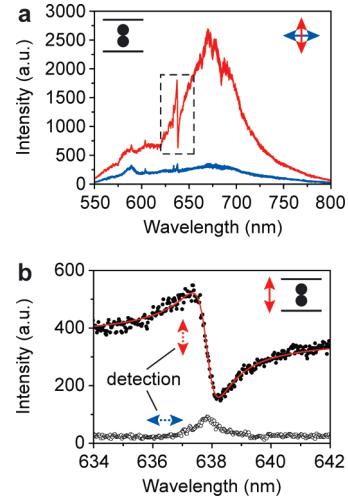

FIGURE 5. (a) Fluorescence spectrum from the configuration shown in Figure 4a (see inset) with the excitation light polarized perpendicular (red) or parallel (blue) to the waveguide axis, respectively. No polarization filtering is applied in the detection path. (b) Resonance peak of mode M1 for the same configuration as in (a). The system is excited along the nanosphere alignment direction and additional polarization filtering perpendicular (filled circles) or parallel (open circles) to the waveguide axis is applied in the detection path. A Fano-type function (red curve, eq 3) is used to fit the data, which was flattened through normalization to the unstructured background prior to fitting.

We adopt a model by Barclay et al.[30] to fit the spectra in Figure 5b and to estimate the coupling efficiency β between the plasmonic and photonic resonance. According to ref 30, the spectral line shape of a point-like emitter coupled to a cavity mode can be described by a function of the form

$$S(\lambda) = A\left|1 + \frac{\xi\sqrt{F_{\text{ph}}\exp(-i\Delta\Phi)}}{1 + 2iQ(1 - \lambda_c/\lambda)}\right|^2 \tag{3}$$

where λ_c is the central wavelength of the cavity mode, $\xi = \xi_c/\xi_d$ is the ratio of the collection efficiencies for radiation from the cavity and for direct emission from the nanoantenna, respectively, $\Delta\Phi = \Phi_d - \Phi_c$ is the phase difference between these two detection pathways, and A is a proportionality constant. From corresponding FDTD simulations of the farfield radiation pattern we deduce a ratio $\xi \approx 1.5$ in the case of mode M1. F_{ph} is the Purcell factor of the photonic resonance and is related to the total Purcell factor F of the hybrid gold-cavity system through $F = F_{\text{ph}}F_{\text{pl}}$, with F_{pl} being the Purcell factor of the plasmonic resonance.[2] Using eq 3, the fit in Figure 5b yields a value $F_{\text{ph}} \approx 0.65$, which translates into a coupling efficiency $\beta = F_{\text{ph}}/(1 + F_{\text{ph}}) \approx 0.4$ between the plasmonic

DOI: 10.1021/nl903555u | Nano Lett. 2010, 10, 891–895

and photonic resonance. This value means that approximately 40 % of the plasmon-enhanced emission from the nanoantenna couples into the cavity mode. Note that such a quantitative analysis is not possible for the nanorod-cavity configuration (Figure 2) discussed earlier, since the signal from the nanorod is too small compared to the incoherent background from the silicon nitride.

Our results prove the general feasibility of a hybrid metal-dielectric cavity system and highlight some of its unique optical properties, such as the strong field localization as well as the extreme polarization sensitivity. The main task in future studies will be to optimize the plasmonic field enhancement as well as the coupling efficiency to the PhC cavity. For example, there is ample room for further improvement by carefully designing the metal nanostructures. The relatively large gold nanorods used here exhibit plasmonic quality factors $Q_{pl} \approx 14$ (determined by single particle dark field spectroscopy,[31] see Figure S2 of the Supporting Information), but smaller rods show corresponding values of up to 22 (ref 21), which can further be improved by ~30 % through additional coating with a thin silver shell.[32] Combining two such nanorods to a dimer (as was done here for gold nanospheres) may then lead to extremely high field enhancements.[33] However, care has to be taken not to degrade the quality factor Q of the hybrid system too much, as a stronger field localization also leads to larger radiative loss. Consequently, a suitable trade-off has to be found, depending on the requirements of the specific application. Future implementations may also use PhC cavities with higher intrinsic quality factors, for example, made from gallium phosphide.[34] Furthermore, ways have to be explored to fabricate these devices using scalable lithographic techniques, as the nanoassembly method employed here (although convenient for studying the underlying physics) is not suitable for large-scale production. Once these issues have been addressed, hybrid plasmonic-photonic cavities may find wide application in integrated opto-plasmonic devices for quantum information processing, as efficient single photon sources or nanolasers, or as sensing elements for surface enhanced Raman scattering.[35]

Acknowledgment. This work was supported by the Deutsche Forschungsgemeinschaft (BE 2224/9 and SFB 448). J.B. acknowledges a scholarship by the Carl-Zeiss foundation.

Supporting Information Available. Optical properties of gold nanorods and various gold-cavity configurations. This material is available free of charge via the Internet at http://pubs.acs.org.

REFERENCES AND NOTES

(1) Barnes, W. L.; Dereux, A.; Ebbesen, T. W. *Nature* **2003**, *424*, 824–830.
(2) Chang, D. E.; Sørensen, A. S.; Hemmer, P. R.; Lukin, M. D. *Phys. Rev. Lett.* **2006**, *97*, No. 053002.
(3) Gong, Y.; Vučković, J. *Appl. Phys. Lett.* **2007**, *90*, No. 033113.
(4) Ditlbacher, H.; Hohenau, A.; Wagner, D.; Kreibig, U.; Rogers, M.; Hofer, F.; Aussenegg, F. R.; Krenn, J. R. *Phys. Rev. Lett.* **2005**, *95*, 257403.
(5) Miyazaki, H. T.; Kurokawa, Y. *Phys. Rev. Lett.* **2006**, *96*, No. 097401.
(6) Weeber, J.-C.; Bouhelier, A.; Colas des Francs, G.; Markey, L.; Dereux, A. *Nano Lett.* **2007**, *7*, 1352–1359.
(7) Hill, M. T.; Oei, Y.-S.; Smalbrugge, B.; Zhu, Y.; de Vries, T.; van Veldhoven, P. J.; van Otten, F. W. M.; Eijkemans, T. J.; Turkiewicz, J. P.; de Waardt, H.; Geluk, E. J.; Kwon, S.-H.; Lee, Y.-H.; Nötzel, R.; Smit, M. K. *Nat. Photon.* **2007**, *1*, 589–594.
(8) Min, B.; Ostby, E.; Sorger, V.; Ulin-Avila, E.; Yang, L.; Zhang, X.; Vahala, K. *Nature* **2009**, *457*, 455–459.
(9) Nozaki, K.; Baba, T. *Appl. Phys. Lett.* **2006**, *88*, 211101.
(10) Coccioli, R.; Boroditsky, M.; Kim, K. W.; Rahmat-Samii, Y.; Yablonovitch, E. *IEE Proc.: Optoelectron.* **1998**, *145*, 391–397.
(11) de Angelis, F.; Patrini, M.; Das, G.; Maksymov, I.; Galli, M.; Businaro, L.; Andreani, L. C.; di Fabrizio, E. *Nano Lett.* **2008**, *8*, 2321–2327.
(12) Barth, M.; Stingl, J.; Kouba, J.; Nüsse, N.; Löchel, B.; Benson, O. *Phys. Status Solidi B* **2009**, *246*, 298–301.
(13) Song, B.-S.; Noda, S.; Asano, T.; Akahane, Y. *Nat. Mater.* **2005**, *4*, 207–210.
(14) Barth, M.; Nüsse, N.; Stingl, J.; Löchel, B.; Benson, O. *Appl. Phys. Lett.* **2008**, *93*, No. 021112.
(15) Barth, M.; Kouba, J.; Stingl, J.; Löchel, B.; Benson, O. *Opt. Express* **2007**, *15*, 17231–17240.
(16) Anderson, M. S. *Appl. Phys. Lett.* **2008**, *92*, 123101.
(17) Merlein, J.; Kahl, M.; Zuschlag, A.; Sell, A.; Halm, A.; Boneberg, J.; Leiderer, P.; Leitenstorfer, A.; Bratschitsch, R. *Nature Photon.* **2008**, *2*, 230–233.
(18) Bek, A.; Jansen, R.; Ringler, M.; Mayilo, S.; Klar, T. A.; Feldmann, J. *Nano Lett.* **2008**, *8*, 485–490.
(19) Schietinger, S.; Barth, M.; Aichele, T.; Benson, O. *Nano Lett.* **2009**, *9*, 1694–1698.
(20) Barth, M.; Nüsse, N.; Löchel, B.; Benson, O. *Opt. Lett.* **2009**, *34*, 1108–1110.
(21) Sönnichsen, C.; Franzl, T.; Wilk, T.; von Plessen, G.; Feldmann, J.; Wilson, O.; Mulvaney, P. *Phys. Rev. Lett.* **2002**, *88*, No. 077402.
(22) Nikoobakht, B.; El-Sayed, M. A. *Chem. Mater.* **2003**, *15*, 1957–1962.
(23) Fano, U. *Phys. Rev.* **1961**, *124*, 1866–1878.
(24) Pinotsi, P.; Imamolu, A. *Phys. Rev. Lett.* **2008**, *100*, No. 093603.
(25) Hao, E.; Schatz, G. C. *J. Chem. Phys.* **2004**, *120*, 357–366.
(26) Purcell, E. M. *Phys. Rev.* **1946**, *69*, 681.
(27) Dulkeith, E.; Niedereichholz, T.; Klar, T. A.; Feldmann, J.; von Plessen, G.; Gittins, D. I.; Mayya, K. S.; Caruso, F. *Phys. Rev. B* **2004**, *70*, 205424.
(28) Rechberger, W.; Hohenau, A.; Leitner, A.; Krenn, J. R.; Lamprecht, B.; Aussenegg, F. R. *Opt. Commun.* **2003**, *220*, 137–141.
(29) Su, K. H.; Wei, Q. H.; Zhang, X.; Mock, J. J.; Smith, D. R.; Schultz, S. *Nano Lett.* **2003**, *3*, 1087–1090.
(30) Barclay, P. E.; Santori, C.; Fu, K.-M.; Beausoleil, R. G.; Painter, O. *Opt. Express* **2009**, *17*, 8081–8097.
(31) Becker, J.; Schubert, O.; Sönnichsen, C. *Nano Lett.* **2007**, *7*, 1664–1669.
(32) Becker, J.; Zins, I.; Jakab, A.; Khalavka, Y.; Schubert, O.; Sönnichsen, C. *Nano Lett.* **2008**, *8*, 1719–1723.
(33) Rogobete, L.; Kaminski, F.; Agio, M.; Sandoghdar, V. *Opt. Lett.* **2007**, *32*, 1623–1625.
(34) Rivoire, K.; Kinkhabwala, A.; Hatami, F.; Masselink, W. T.; Avlasevich, Y.; Müllen, K.; Moerner, W. E.; Vučković, J. *Appl. Phys. Lett.* **2009**, *95*, 123113.
(35) Anker, J. N.; Hall, W. P.; Lyandres, O.; Shah, N. C.; Zhao, J.; van Duyne, R. P. *Nat. Mater.* **2008**, *7*, 442–453.

DOI: 10.1021/nl903555u | *Nano Lett.* **2010,** *10,* 891–895